Raman Spectroscopy of Pentaerythritol Single Crystals under High Pressures

Ta-Ryeong Park,† Zbigniew A. Dreger,* and Yogendra M. Gupta

Institute for Shock Physics and Department of Physics, Washington State University, Pullman, Washington 99164-2816

Received: October 21, 2003

The effect of pressure on the Raman spectra of pentaerythritol (PE) single crystals was examined up to 10 GPa. Several abrupt changes in the spectra were found at 4.6 ± 0.2 GPa and 6.8 ± 0.3 GPa. These changes occur both in the internal and external modes and indicate the onset of phase transitions. Both transitions demonstrate considerable pressure hysteresis characteristic of a first-order phase change. It is concluded that PE crystals can exist in three different phases in the pressure range up to 10 GPa. Phase I, which has the bct structure, extends up to 4.6 GPa. In phase II, the number of translationally nonequivalent molecules in a PE unit cell is likely doubled. Phase III, above 6.8 GPa, has features of a disordered structure and is associated with a large softening of hydrogen bonding.

I. Introduction

Vibrational spectroscopy under high pressures provides a useful method to examine and understand the effects of intermolecular interactions on the stability of molecular crystal structures. Changes in the vibrational spectra can be utilized for probing modifications in lattice dynamics, molecule arrangements, and/or molecule conformations.[1,2] Here, we report the effects of pressure on the Raman spectra of pentaerythritol (PE) single crystals. Pentaerythritol (2,2-bis(hydroxymethyl)-1,3-propanediol, $C(CH_2OH)_4$) is a simple solid polyalcohol formed by the combination of the van der Waals (vdW) forces and hydrogen bonding (HB). The latter, at ambient conditions, forms a regular quasi-planar and quadrilateral network.[3−5] Owing to its relatively simple structure, PE can be considered as a model system for studying the structure and phase stability of hydrogen-bonded molecular solids.

At ambient conditions, PE molecules possess S_4 symmetry and crystallize in the body-centered tetragonal (bct) structure belonging to the $I\bar{4}$ space group.[3−9] The primitive unit cell contains only one molecule, and the factor group, site and molecular symmetry are the same, S_4. As shown in Figure 1a, the skeleton of the PE molecule consists of two intersecting all-trans O−C−C−C−O chains that share their central atoms in a tetrahedral arrangement. The PE molecule is relatively flexible, and its fragments can rotate about the C−C or C−O single bonds. As a result, the isolated PE molecule maintains the minimum energy when the angle between the O−H and O−C bonds reaches 180°. In contrast, in the crystalline environment this angle becomes 90°, which is the least stable conformation for a free PE molecule.[4] Therefore, the conformation assumed by the PE molecule in the crystal is mainly due to intermolecular forces, the strongest of which are the hydrogen bonds linking the molecules into layers along the (001) planes (Figure 1b). In this arrangement each hydroxyl group is involved in two hydrogen bonds of 2.71 Å (O···O distance), and eight symmetry equivalent hydrogen bonds that link one molecule with four neighboring molecules. The cohesion forces between the layers are the relatively weak van der Waals type interactions. The perfect cleavage normal to the [001] axis is accounted for by such a layer structure. Although the intermolecular forces along the [001] direction are much weaker than the hydrogen bonds within the (001) layers, the arrangement of the centers of the molecules approximates a cubic lattice. At temperatures higher than ∼462−464 K,[10,11] PE was found to transform to an orientationally disordered, face-centered cubic (fcc) structure. In this phase the PE molecules can rotate about the C−C bonds, and the layer structure of the tetragonal form is no longer retained. It was proposed that the disordered structure approaches nearly the $F\bar{4}\,3m$ space group.[12]

Only a few studies have been reported on the high-pressure response of pentaerythritol,[5,13−15] prior to the start of our work. Furthermore, these studies were performed over a very limited pressure range, up to about 1 GPa. Discontinuities in the lattice parameters at ∼0.5 GPa were observed by using X-ray powder diffraction measurements and were interpreted as revealing a first-order phase transition.[12,13] However, these findings were not confirmed by the latest studies on single crystals, where no evidence of a phase transition was found up to 1.15 GPa.[5] After completing this work, we came across a paper on high-pressure Raman studies.[16] The paper reports pressure effects on PE powder up to 25 GPa. On the basis of internal modes changes, three pressure-induced phase transitions were suggested at 6.3, 8.2, and 10 GPa. It was proposed that the high-pressure phases could result in lowering of crystalline symmetry. In summary, previous studies provide scarce and often contradicting information on the behavior of PE crystals under high pressure. Hence, the question concerning the pressure-induced phase transitions in pentaerythritol crystal remains an open one. To mitigate some of the problems apparently encountered in previous studies (random morphology of samples and uncertain compression conditions), the experiments reported here were performed with good quality single crystals and under well-controlled pressure conditions.

The present studies were undertaken to provide detailed data, over a broad range of pressures (up to 10 GPa), on both internal and external vibrational modes of PE crystals to identify the factors that may destabilize the ambient structure and also to verify the information regarding the suggested pressure-induced phase transitions. Besides, we believed that the competition

* Corresponding author. E-mail: dreger@wsu.edu.

† On sabbatical leave from the Department of Physics, Hoseo University, Asan, Choongnam 336-795, Korea.

10.1021/jp031179d CCC: $27.50
Published on Web 02/13/2004

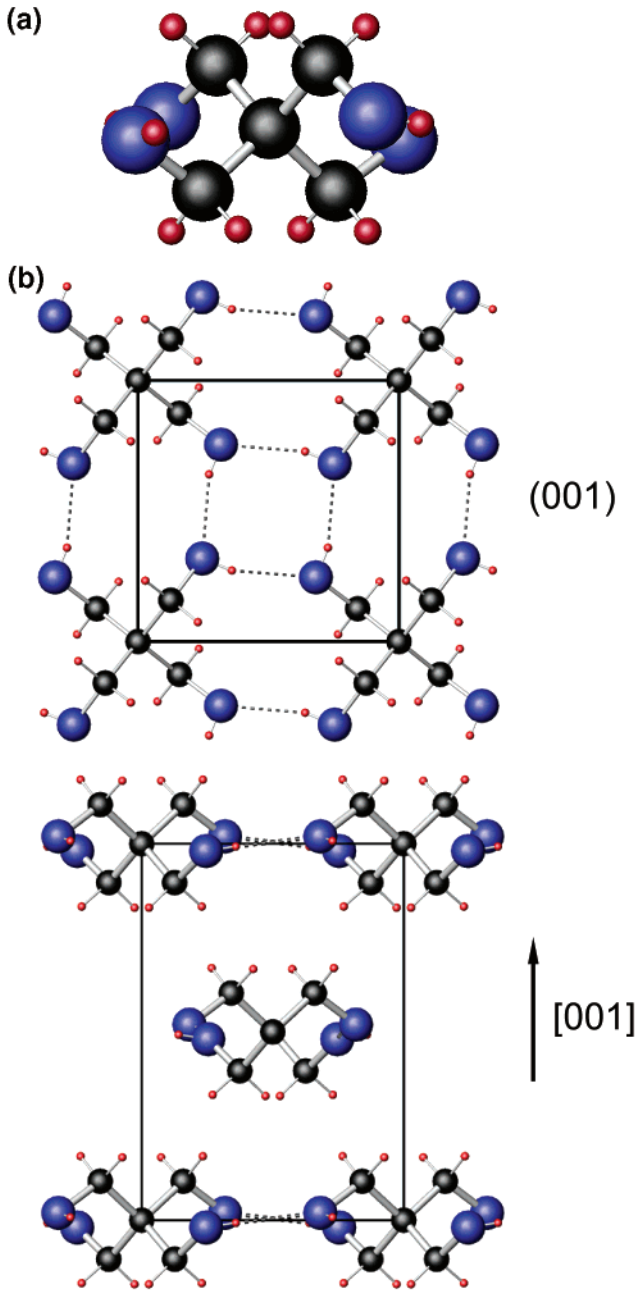

Figure 1. (a) Ball-and-stick model of the S_4 conformer, which the PE molecule assumes in the crystal at ambient conditions. The projection of the molecule compatible with the *ac* plane is shown. Legend: carbon, black; oxygen, blue; hydrogen, red. (b) Crystal structure of PE. Top: view of molecules sited on the (001) plane. Bottom: view along crystallographic *c* axis. The hydrogen bonds are delineated by dashed lines. The unit cell is demarcated by solid lines.

between the vdW and HB interactions could be altered by pressure, which may potentially lead to structural transitions. Experimental studies of such transitions are expected to be useful in understanding the transition mechanisms, structural relations among various phases, and in the identification of new phases.

The remainder of the paper is organized as follows. Experimental procedures including sample preparation, high-pressure generation, and Raman measurements are described briefly in the next section. Section III presents the experimental data regarding the pressure dependence of the internal and external vibrations. In section IV we discuss the implications of pressure-induced changes on the Raman spectra of PE. The main findings of this work are summarized in Section V.

II. Experimental Procedure

Pentaerythritol of 99+% purity was purchased from Sigma-Aldrich and used without further purification. Optical quality PE single crystals were grown by slow cooling of saturated aqueous solutions. In general, the crystals had shapes of tetragonal pyramids with approximate dimensions of $5 \times 5 \times 4$ mm^3. The large crystals were suitably cleaved or cut into small pieces for high-pressure experiments. Two types of samples were prepared: one cleaved along the (001) plane and the other cut perpendicular to this plane. Use of these two orientations allowed an examination of the vibrational modes having different symmetry. Typical lateral dimensions of experimental samples were about 0.12×0.1 mm^2 with a thickness of $\sim$0.03 mm.

High pressures were generated in a modified Merrill−Bassett type diamond anvil cell (DAC). Either Inconel or stainless steel gaskets, preindented to 0.1 mm with a 0.2 mm hole drilled in the indentation, were used as a sample compartment. A 4:1 methanol/ethanol mixture or cryogenically loaded nitrogen was used as a pressure-transmitting medium. The same results were obtained in both media. The ruby calibration method was used to monitor the pressure.[17] A small chip of ruby, placed inside the gasket aperture with the PE crystal, was excited with a 532 nm line from a diode-pumped solid-state laser (DPSSL, Crystalaser). The resulting fluorescence was dispersed by a 0.22 m double spectrometer (Spex 1680) and detected using an air-cooled charge-coupled device (CCD) (Princeton Instruments). Pressure was determined from the frequency shift of the ruby R_1 fluorescence line. By monitoring the separation and widths of both R_1 and R_2 lines, we confirmed that hydrostatic conditions were maintained throughout these experiments. The precision of our pressure measurements is estimated to be 0.05 GPa.

The 514.5 or 457.9 nm lines from a CW Ar-ion laser (Innova 90, Coherent) were employed for Raman excitation. Less than 100 mW of power was incident on the sample. The scattered signal was collected in a backscattering geometry and dispersed using a 0.6 m triple spectrometer (Spex 1877) and recorded on a liquid-N_2-cooled CCD (Princeton Instruments). The estimated resolution of the system was about 1 cm^{-1}. All the experiments were carried out at room temperature and were repeated several times using different samples to check the consistency of the data. Raman spectra were measured both during pressure loading and release. Pressure-induced shifts of overlapping bands were analyzed by fitting the Raman spectra to Gaussian−Lorentzian components using a nonlinear least-squares algorithm. Experimental details regarding Raman and fluorescence techniques can be seen elsewhere.[18]

In addition, optical images of the samples were taken to complement the spectroscopy measurements. These images were acquired using a microscope equipped with a 50× LWD (long working distance objective, Mitutoyo) and a color CCD (Diagnostic Instruments).

III. Results

III.A. Ambient Pressure. Group theory predicts 60 fundamental vibrations for PE crystals divided as follows: internal, $\Gamma_{int} = 14A + 15B + 14E$, and external, $\Gamma_{ext} = A + E$, modes. All vibrations are Raman-active and most of them have sufficient intensity to be detected in our experiments. In Figure 2, we show the Raman spectra of a PE single crystal at ambient pressure. The peaks represent the internal modes occurring over the entire range of the PE Raman activity (150−3500 cm^{-1}). The spectra are unpolarized but the incident light was polarized normal to the [001] crystal axis. For this orientation the modes

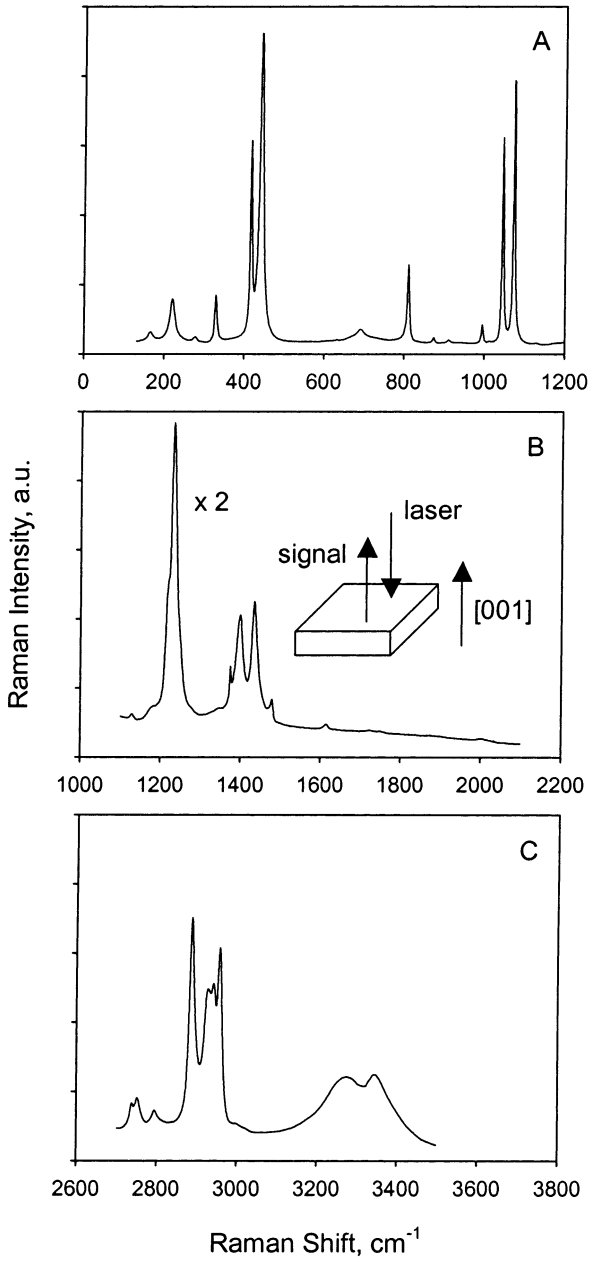

Figure 2. Raman spectra of the PE crystal representing internal modes in three frequency regions. The spectra are obtained at atmospheric pressure for the crystal orientation shown in the inset. For all frequency regions the same scale is adopted to reveal the relative intensities and widths of different modes. In graph B, the Raman intensity is multiplied by 2.

of E-symmetry are not observed. The ambient pressure Raman spectra agree well with those reported previously, using Raman,[19] IR,[20] and calculations.[21] Because the CH and OH modes located between 1300 and 1400 cm^{-1} interfere with the diamond mode at 1330 cm^{-1} they were not examined in detail under pressure.

III.B. Pressure Effects: Internal Vibrations. Figure 3 shows typical Raman spectra at several pressures in the frequency range 150−1300 cm^{-1}. The spectra were obtained for increasing pressures from 1 atm to 10 GPa with the laser beam parallel to the [001] crystal direction. With increasing pressure, all modes shift gradually toward higher frequencies. However, at ∼4.6 GPa the spectrum suddenly changes, displaying several new features. The most pronounced one is the splitting of the CO-stretching mode located at 1043 cm^{-1}, under

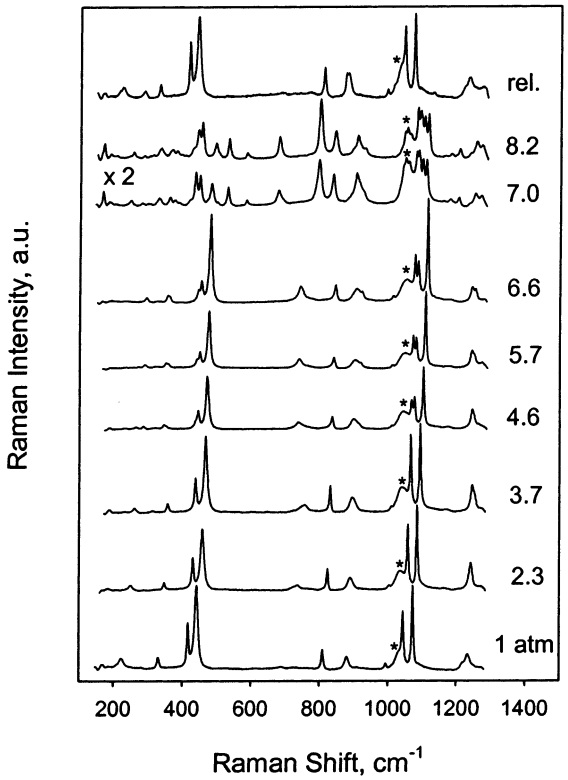

Figure 3. Raman spectra of PE in the frequency range of 150−1300 cm^{-1} at several pressures. The curves in this figure are vertically displaced for the sake of clarity. Pressure values are shown in GPa next to each spectrum. The asterisks indicate a peak from the pressure-transmitting medium. The Raman spectra intensity at 7.0 and 8.2 GPa is multiplied by 2. The spectra were obtained with the laser beam parallel to the [001] crystal direction.

ambient conditions. With further increase of pressure, the spectrum remains essentially similar to that at 4.6 GPa. This continues until ∼6.8 GPa, above which the spectrum undergoes a drastic transformation. The changes at this pressure include the following: a significant decrease in the Raman intensity, multiple splitting, and a discontinuity in shifts of existing modes. Despite the complexity of these changes, the sample-to-sample reproducibility of the spectrum above 6.8 GPa was quite good. The pressure-induced changes were fully reversible as indicated by the released spectrum (top trace in Figure 3). Two additional peaks observed in this spectrum at 306 and 1133 cm^{-1}, both of E-symmetry, arise apparently as a result of the changed crystal orientation in the cell upon decompression. The feature labeled with an asterisk represents the band from the methanol/ethanol (M/E) mixture.[22−24] Also, the peak at ∼878 cm^{-1} is composed of the PE mode at 877 cm^{-1} and a weak band of M/E.

The "transition" pressures were quite reproducible to within ± (0.2−0.3) GPa. Once these pressures were attained, the changes in the spectrum evolved and were completed within 20−30 min. In Figure 4, we compare in detail the spectra for three distinct pressure ranges: below 4.6 GPa, phase I; between 4.6 and 6.8 GPa, phase II; and above 6.8 GPa, phase III. First, it is evident that several new peaks emerge above 4.6 GPa. The proximity of the new peaks to the original ones indicates that the original peaks are splitting. It is noticeable that the splitting occurs only in the form of doublets. Essentially, there is no peak that splits into three or more peaks. The apparent increase in the number of peaks by more than a factor of 2 in the vicinity of the ν_2 mode is not an indication of multiple splitting. Instead, it is caused by the emergence of modes that were present near the ν_2 mode at ambient conditions but could not be monitored

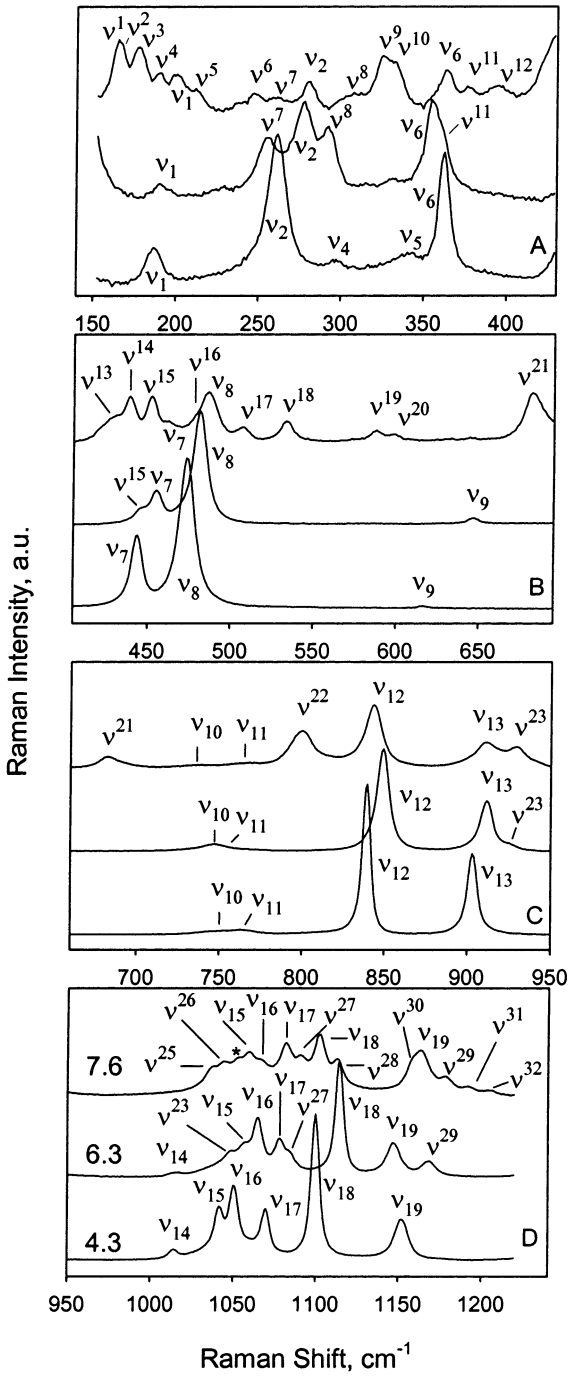

Figure 4. Detailed changes in Raman spectra at selected pressures (4.3, 6.3, and 7.6 GPa), typical for three pressure phases of PE. The intensity of the Raman signal at 7.6 GPa is multiplied by a factor of 1, 3, 2, and 2, respectively for graphs A, B, C, and D. Note that the modes existing at atmospheric pressure are denoted with subscripts, whereas new modes are denoted with superscripts. The feature labeled with an asterisk represents a band of the methanol/ethanol mixture. The spectra were obtained with the laser beam normal to the [001] crystal direction.

under pressure because of their low intensity. The splitting occurs not only with the doubly degenerate modes (ν_{13}, ν_{15}, and ν_{19}) but also with nondegenerate modes (ν_2, ν_6, ν_7, and ν_{17}). Because the nondegenerate modes split, lowering of the molecular symmetry alone cannot be the cause of the observed splitting.

In addition to the splitting, most of the modes display a clear discontinuity and/or a change in the slope at ~4.6 GPa. These features can be seen in parts a−d of Figure 5 that represent the pressure dependence of the mode frequencies located between 150 and 1200 cm^{-1}. All modes shift gradually up to 4.6 GPa, with no indication of any irregularities in the low-pressure range, particularly around 0.5 GPa, as implied in ref 16. For most of the modes, the slope dν/dp (pressure coefficient) decreases with increasing pressure. Slope values, at selected pressures, were obtained from the least-squares fits of the experimental data to either a polynomial or a linear equation. Table 1 includes the calculated coefficients together with the mode assignments and their frequencies. As shown, a typical value of dν/dp varies between 4 and 7 cm^{-1} GPa^{-1}. However, the OH-torsion modes (ν_{10}, ν_{11}) display coefficients 3 times larger than any other mode in this frequency region. When the pressure approaches 4.6 GPa, some modes show a much smaller shift. This feature is clearly observed for the CCO-torsion mode (ν_1), the lowest internal mode, which shows no shift after passing ~4 GPa. At 4.6 GPa many of the modes split or show discontinuity in their shifts. The frequencies of the ν_1, ν_6, ν_{10}, ν_{11}, ν_{14}, and ν_{19} modes decrease at the transition, indicating a softening of the structure.

Above ~4.6 GPa, the rate of frequency shift decreases in almost every case. For example, a number of modes, ν^7, ν_{14}, and ν_{19}, show almost no shift over the entire range of 4.6−6.8 GPa. The symbols with subscripts denote the modes present at ambient pressure, whereas the symbols with superscripts denote the modes that emerge at high pressures.

As already mentioned, pressure increase above ~6.8 GPa brings about numerous changes in the spectra. Details of these changes can be seen in Figures 4 and 5a−d. In addition to an overall significant reduction of intensity, the vibrational structure becomes filled with many new peaks. Most of the new peaks occur around the modes already present at lower pressures. The largest buildup of new modes is observed in the vicinity of ν_1, ν_7, ν_8, and ν_{19}. For instance, the ν_1 mode is surrounded by as many as five new peaks. The ν_{19} mode, which splits in phase II, is surrounded by three more components in phase III. It is noticeable that the pressure dependence of this mode in phase III is exactly the same as in phase I. It shifts with the same rate of 4.4 cm^{-1} GPa^{-1} and along the same line in both phases despite the fact that it shows no shift in phase II (see Figure 5d). It appears that many modes in phase III have larger shifts than those in phase II.

In contrast to the other two phases, the modes in phase III show considerable broadening (see Figure 4). One possible source of this line width broadening in the high-pressure experiments is a pressure gradient in the sample. Such a pressure gradient would mean that the molecules would experience slightly different pressures depending on their location within the pressure cell. As can be seen in Figure 6, the broadening occurs mainly across the boundary of phase II and phase III. The broadening extent and its progress with pressure differ among various modes. This would imply that the increase in line widths is likely due to the distribution in arrangement and distortion of different bonds in the molecules, rather than the pressure gradients in the cell. The lack of broadening in the ruby lines supports this statement.

Upon a decrease in pressure, the Raman spectra regain their intensity and shape. However, the frequency shift clearly displays a pressure hysteresis. As can be seen in parts a−d of Figure 5, the transition from phase III to phase II occurs at a pressure that is about 1.2 GPa lower than the value during increasing pressure. Also, the transition from phase II to phase I occurs at ~4 GPa which is 0.6 GPa lower than the value obtained for increasing pressure. These features are characteristic of first-order transitions.

TABLE 1: Pressure Effect on Selected Vibrational Mode[a]

			1 atm				
					high pressure $d\nu/dp$[e] cm^{-1} GPa^{-1} (± 0.3)		
mode	assignt[b]	initial sym[b]	freq calcd[b] cm^{-1} (± 2)[d]	freq exptl[c] cm^{-1} (± 2)[d]	phase I	phase II	phase III
ν_{L1}	lattice	E	74.4	78	13.9; 8.4	4.6	4.4; 1.4
ν_{L2}						4.0 4.2; 0.7	
ν_{L3}							2.4
ν_{L4}							5.7; 2.4
ν_1	CCO t	A	166.0	165	5.4; 0.0	4.5	6.4
ν^1							2.5; 1.2
ν^2							3.7
ν^3							7.3; 4.7
ν^4							7.6; 5.1
ν^5							7.0; 3.0
ν_2	CC tw (skl)	B	220.2	221	14.1; 4.8	6.3	4.7
ν^6							6.8
ν^7						1.0	7.4; 3.6
ν_3	CCO t	E	232.2	233	u/d		
ν^8						4.2	9.7; 5.0
ν_4	CCO t	B	267.2	271	u/d		
ν_5	CCO b	E	309.0	306	u/d		
ν^9							5.1
ν^{10}							9.2; 3.6
ν_6	CCO b	B	332.9	330	8.6; 6.5	5.0	7.8
ν^{11}						5.0	4.9
ν^{12}							7.7
ν^{13}							7.7; 4.6
ν^{14}							7.8; 3.2
ν^{15}						3.9	6.2
ν_7	CCO b	A	424.2	418	6.3; 5.6	3.3	7.5; 3.6
ν_8	CCC b (skl)	A	447.9	443	8.0; 6.0	4.1	9.6; 13.3
ν^{16}						14.1; 4.7	
ν^{17}							4.6
ν^{18}							2.5
ν^{19}							1.5
ν^{20}							2.2
ν_9	CCC b (skl)	E	590.2	592	7.5; 3.6	11.1; 5.3	
ν^{21}							1.9
ν_{10}	OH t	E	680	665	21.6; 15.9	3.1	8.0
ν_{11}	OH t	A	693.2	674	25.2; 15.6	4.0	15.6
ν^{22}							4.3
ν_{12}	CC st (skl)	A	820.6	814	6.5; 4.6	3.8	6.5
ν_{13}	CH r	E	879.2	877	6.9; 4.7	4.7	4.7; 1.8
ν^{23}						4.8	5.1; 3.2
ν_{14}	CCC b (skl)	B	994.7	995	4.6	1.4	
ν^{24}							4.5
ν^{25}							2.6
ν^{26}							4.4
ν_{15}	CO st	E	1016.0	1015	6.1	5.5	4.6
ν_{16}	CH r	B	1006.8	1033	4.1	5.3	4.0
ν_{17}	CO st	B	1047.5	1043	6.1	4.3	4.5
ν^{27}							4.1
ν^{28}							5.0
ν_{18}	CO st	A	1084.6	1075	5.8	4.8	4.8
ν_{19}	CC st (skl)	E	1138.9	1133	4.4	0.7	4.4
ν^{29}							3.2
ν^{30}						3.8	3.6
ν^{31}							3.4
ν^{32}							3.4
ν_{20}	CH st (sym)	B	2758.9	2737	5.0	2.8	
ν_{21}	CH st (sym)	E	2827.7	2752	6.7	3.2	
ν_{22}	CH st (sym)	A	2872.8	2796	5.6	2.9	
ν^{33}	u/d			2877	5.6	2.2	2.5
ν_{23}	CH st (asym)	B	2971.7	2927	4.9	4.6	2.9
ν_{24}	CH st (asym)	E	2972.2	2942	6.0	4.7	6.0
ν^{34}						1.9	0.6
ν_{25}	CH st (asym)	A	2975.3	2957	12.2	6.4	8.6
ν_{26}	OH st	A	3277.1	3274	−49.3; −15.2[f]	−3.0 −3.3	
ν_{27}	OH st	B	3342.7	3345	−31.7; −22.5[f]	−3.6 −4.3	

[a] The pressure effects on the CH and OH modes in the range of 1200 to 1600 cm^{-1} were not examined in detail. [b] Reference 19. [c] This work. [d] The error includes the contribution from the averaging of results from several experiments. [e] The values of the pressure coefficients are obtained from the least-squares fits of the experimental data to either a polynomial or linear equation. The two values in the column correspond to the coefficients, respectively, at the beginning and the end of the particular pressure range. [f] These values are at 4 GPa; t = torsion; tw = twist; skl = skeletal; b = bend; st = stretch; r = rock; sym = symmetric; asym = asymmetric; u/d = undetermined.

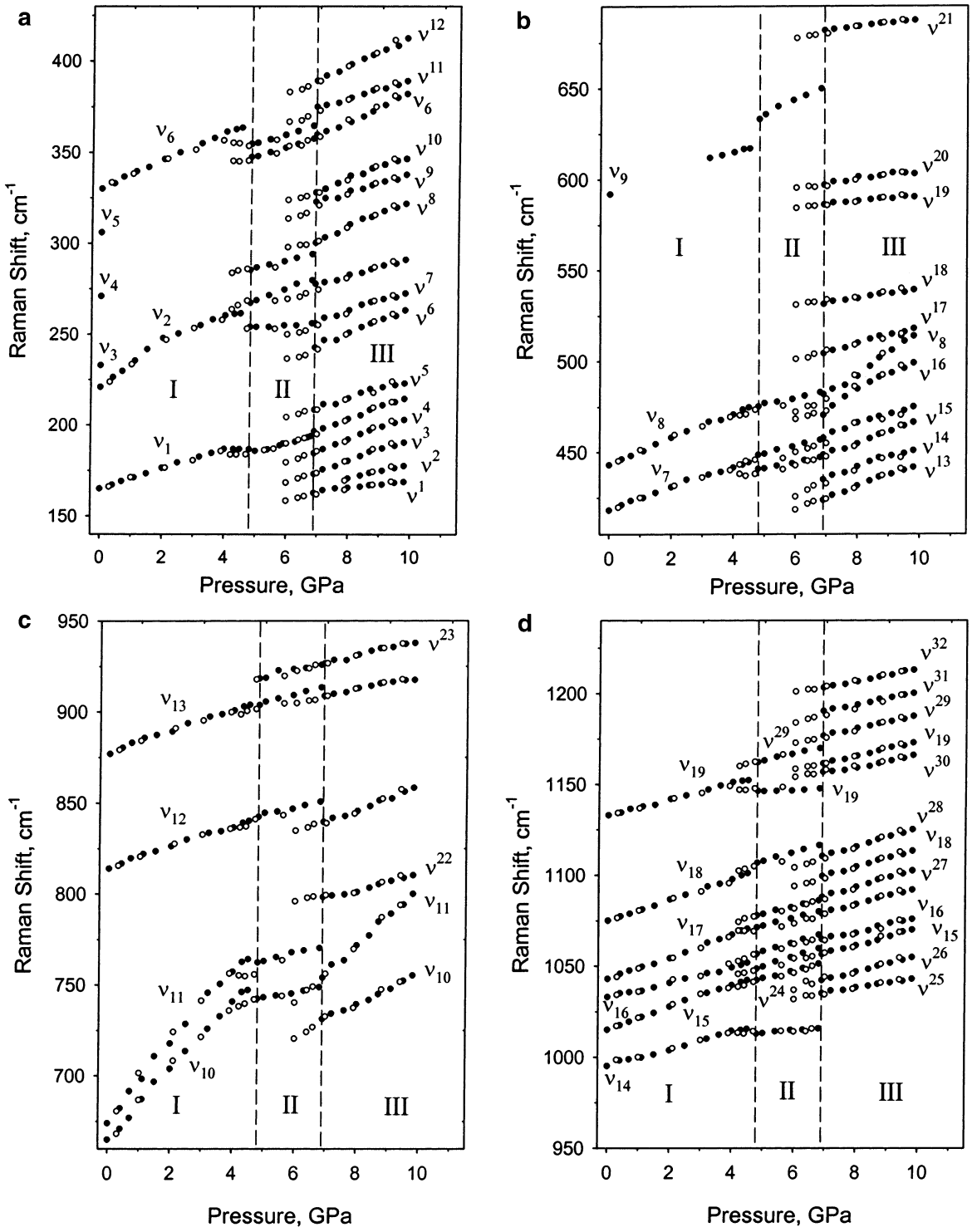

Figure 5. (a) Pressure-induced shifts of the CCO-torsion and -bending modes (ν_1 and ν_6) and the CC-twisting mode (ν_2). Solid symbols represent the shift upon an increase of pressure, whereas open circles represent the shift upon a decrease of pressure. Symbols with superscripts stand for the modes occurring at high pressures. The vertical dashed lines mark the onsets of discontinuities. The roman numbers label different pressure phases. (b) Pressure-induced shifts of the CCO-bending mode (ν_7) and the CCC-bending modes (ν_8 and ν_9). Further explanations as in part a. (c) Pressure-induced shifts of the OH-torsion modes (ν_{10} and ν_{11}), the CC-stretching mode (ν_{12}), and the CH-rocking mode (ν_{13}). Further explanations as in part a. (d) Pressure-induced shifts of the CCC-bending mode (ν_{14}), the CO-stretching modes ($\nu_{15,}$ ν_{17} and ν_{18}), the CH-rocking mode (ν_{16}), and the CC-stretching mode (ν_{19}). Further explanations as in part a.

In Figure 7 we show typical spectra of the CH- and OH-stretching modes under several pressures. It can be noticed that the CH-stretching modes behave similarly to the CH-rocking mode at 877 cm^{-1} (see Table 1). They shift at an average of 6 cm^{-1} GPa^{-1} in phase I and 3−4 cm^{-1} GPa^{-1} in phase II. One new peak, ν^{34}, emerges above 4.6 GPa, and subsequently it shows almost no pressure dependence. In phase III, all CH symmetric modes are no longer detected. In general, the spectra in the CH-stretching region are less susceptible to pressure than the spectra in the low-frequency range.

Our results are somewhat different from those recently published by Bhattacharya and Sharma,[16] who found pressure-induced phase transitions at 6.3, 8.2, and 10 GPa. However, their reported spectra showed low resolution with relatively

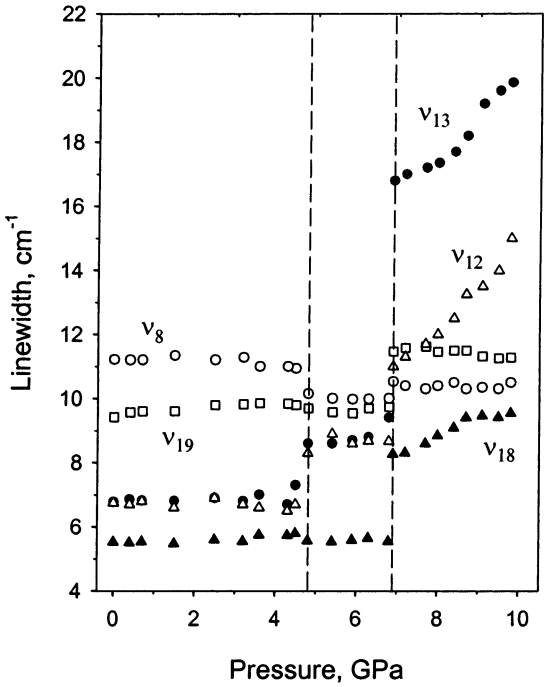

Figure 6. Pressure effect on the line width of selected internal modes: ν_8 (CCC-bending), ν_{12} (CC-stretching), ν_{13} (CH-rocking), ν_{18} (CO-stretching), and ν_{19} (CC-stretching).

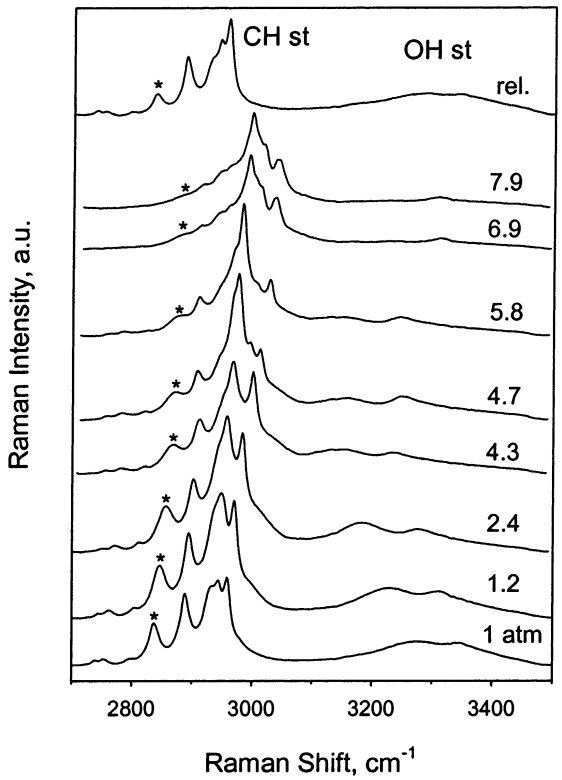

Figure 7. Effect of pressure on the CH- and OH-stretching modes. Pressure values are shown in GPa next to each spectrum. The curves in this figure are vertically displaced for the sake of clarity. The feature labeled with an asterisk represents a band of the methanol/ethanol mixture. The spectra were obtained with the laser beam parallel to the [001] crystal direction.

broad lines. The discrepancy may originate in the different experimental conditions present in the two studies. While we used high-purity single crystals in hydrostatic media, the authors of ref 16 used low-purity, 97%, powder samples compressed

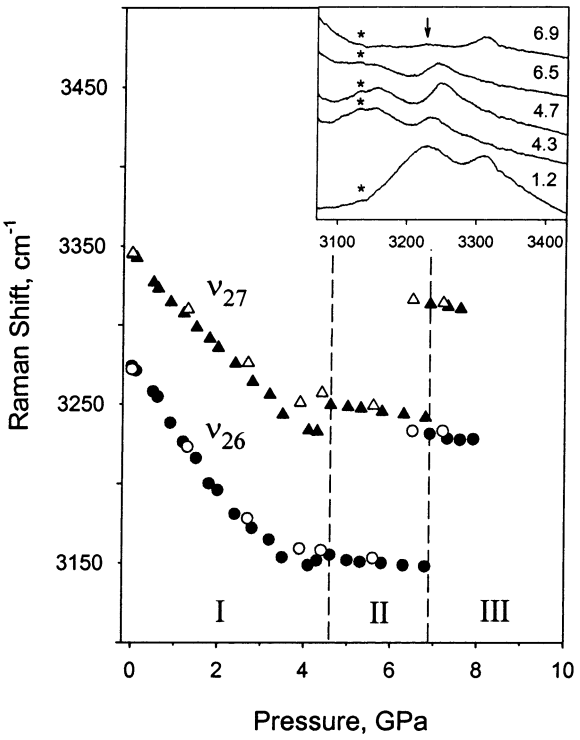

Figure 8. Pressure-induced shift of the OH-stretching modes. Solid symbols represent the shift upon an increase of pressure, whereas open symbols represent the shift upon a decrease of pressure. Circles and triangles represent modes of A- and B-symmetry, respectively. The changes in shape and intensity of these modes are shown in the inset. The intensity of the spectrum at 6.9 GPa is multiplied by a factor 1.5.

without any pressure-transmitting medium. It is known that under these conditions the sample may experience pressure gradients that may result in different transition pressures compared to those under hydrostatic conditions. The apparent broadening of the Raman modes under pressure for powder samples may indeed indicate inhomogeneous conditions.

III.C. Pressure Effect: Hydroxyl (OH) Group Vibrations. Because the hydroxyl groups are involved in hydrogen bonding, their vibrations are of primary importance for probing the changes in intermolecular interactions. Three types of OH vibrations arise in a PE crystal: torsion (~700 cm^{-1}), deformation (~1400 cm^{-1}), and stretching (3250−3350 cm^{-1}). As shown in section III.B., the OH-torsion modes, ν_{10} and ν_{11}, exhibit exceptionally strong pressure dependence in phase I, somewhat smaller dependence in phase III, and only modest dependence in phase II (see Figure 5c). A significant discontinuity in mode frequencies accompanies the changes between different phases. Given that the OH-deformation modes overlap with the diamond peak, they were not followed under pressure.

Two broad OH-stretching modes are located at 3274 cm^{-1} (ν_{26}, A-symmetry) and 3345 cm^{-1} (ν_{27}, B-symmetry) at ambient conditions. Because, the typical frequency of the OH-stretching vibrations in the absence of hydrogen bonding (HB) occurs around 3500−3600 cm^{-1}, the above values are lowered by the presence of HB in the crystal.[25] As can be seen in Figures 7 and 8, the OH-stretching modes demonstrate several notable features under pressure. First, in contrast to all other modes, the frequencies of OH-stretching vibrations decrease with pressure. This effect was observed previously with other hydrogen-bonded compounds and can be attributed to an increase in the OH···O hydrogen bond strength under pressure.[26−28] In phase I, both modes, ν_{26} and ν_{27}, shift strongly to lower frequencies within the first 4 GPa. However, above 4

GPa the rate of the shift significantly slows down, prior to the frequency jump at 4.6 GPa. The frequency decrease continues in phase II, although at a lower rate. It appears that the shift in phase II reduces the entire frequency gain acquired at 4.6 GPa. When the pressure reaches ~6.8 GPa, there is a second discontinuity (~80 cm^{-1}) that increases the ν_{26} and ν_{27} frequencies to the values close to those assumed at ambient pressure. However, the intensity of these modes, particularly ν_{26}, diminishes drastically. The pressure-induced shifts in phase III demonstrate nearly the same negative slopes as in phase II. The combination of low intensity and broad shape for both modes made it impossible to determine their shift above 8 GPa. Upon a release of the pressure, the shifts in OH-stretching modes show hysteresis similar to other modes. Complete release of pressure brings the spectra back to the original location and shape.

III.D. Pressure Effect: External (Lattice) Vibrations. The external modes of the pentaerythritol crystal comprise two acoustic and two lattice vibrations, in each case, one of A- and the other of E-symmetry. The acoustic modes are not observed with Raman spectroscopy since their frequencies approach zero for the wave vector → 0. The lattice mode A represents the libration of the molecule about the *Z*-axis, whereas the E-mode represents the libration about the *X* or *Y* crystal axes. At ambient conditions these modes are theoretically expected to occur at 46.4 cm^{-1} (A-mode) and 74.4 cm^{-1} (E-mode).[21] As in previous studies,[19,20] we were able to detect only the E-mode. It was found at 78 cm^{-1}, with the laser beam normal to the [001] crystal direction. The pressure evolution of this mode, denoted as ν_{L1}, and the lowest internal modes are presented in Figure 9. Under pressure the lattice mode shows substantial blue shift with a large increase in intensity. At the same time, the lowest internal mode, ν_1, shifts less and its intensity decreases significantly. Thus, the frequency gap between ν_{L1} and ν_1 decreases from 87 cm^{-1} at ambient pressure to 57 cm^{-1} at 4.6 GPa. Above 4.6 GPa a new peak, indicated by ν_{L2}, appears on the low-frequency side of the E-mode. Because all the internal modes of PE occur with frequencies higher than 165 cm^{-1}, this new mode is apparently an external mode. It should be mentioned that, unlike the E-mode (ν_{L1}), the ν_{L2} mode was also detected with a laser beam parallel to the [001] direction. However, the intensity of ν_{L2} in the latter case was much lower than in the former one. As shown in Figure 10, the lattice mode ν_{L1} makes shifts continuously at the transition pressure. However, its width in phase II increases gradually from 10.5 cm^{-1} to about 13.5 cm^{-1}, apparently as a result of the splitting of the ν_{L1} mode. Both modes, ν_{L1} and ν_{L2}, shift with comparable rates in phase II. Above ~6.8 GPa, Raman intensity in the low-frequency range diminishes drastically and two well-defined external modes disappear. Instead, several weak peaks can be isolated from a strong background. In Figure 9, the intensity of spectra in phase III are multiplied by 3. This rather complex pattern of peaks in the low-frequency region is preserved up to 10 GPa, the highest pressure applied in our work. The origin of these small peaks, distributed between ~100 and ~200 wavenumbers, is not clear. However, it seems that they are grouped in two spectral regions corresponding to the location of external modes, ν_{L1} and ν_{L2}, and internal mode, ν_1, in phase II. On the basis of the location criterion, we tentatively assign the four lowest peaks as external modes and the five others as internal modes. Pressure-induced shifts of these modes are shown in Figures 5a and 10, respectively, for internal and external modes. The latter ones display similar pressure dependences as those of modes ν_{L1} and

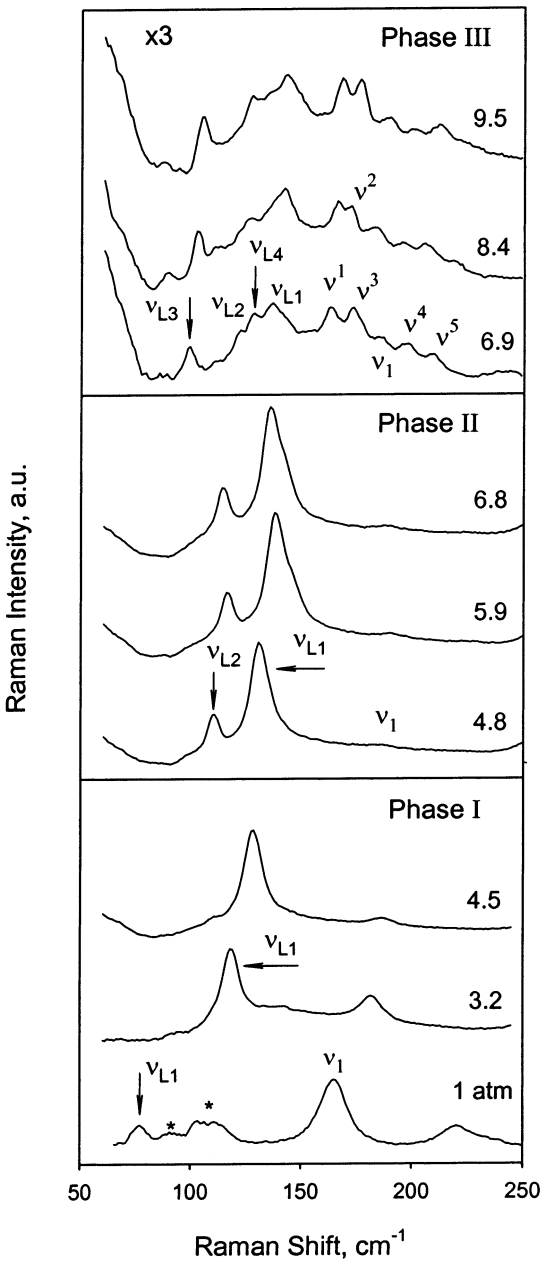

Figure 9. Effect of pressure on external modes and lowest internal modes. External modes are denoted with subscript L. Pressure values are shown in GPa next to each spectrum. In phase III the Raman intensities are multiplied by 3. The features labeled with an asterisk represent peaks from diamonds. The spectra were obtained with the laser beam normal to the [001] direction.

ν_{L2} in phase II. It is worth noticing that some internal modes, for example, ν^3, ν^4, and ν^5, shift stronger with pressure than the external modes. The changes in the region of the external modes are reversible upon pressure release. However, like internal modes, they clearly show a hysteresis in their pressure evolution. As seen in Figure 10, transitions between different phases take place at lower pressure during decreasing pressures than increasing pressure.

In Figure 11 we present typical images of PE sample in the high-pressure cell. The pictures shown are the views of the (001) crystal plane at several pressures. A number of features are observed that apparently coincide with changes in the Raman spectra. First, several lines occur on the sample surface above ~4.6 GPa. Though the extent and concentration of these lines varied from experiment to experiment, they were always

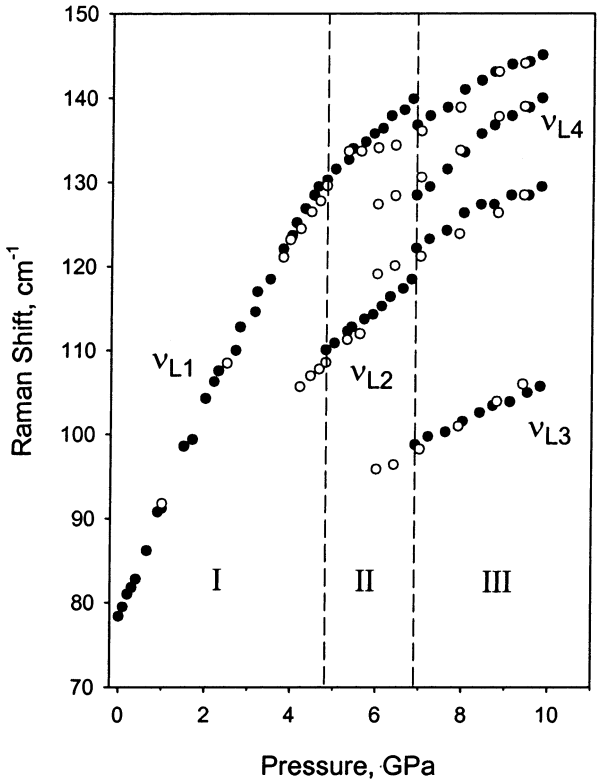

Figure 10. Pressure-induced changes in external modes. Dashed lines are drawn to denote the onsets of discontinuity. Solid symbols represent the shift upon an increase of pressure, whereas open circles represent the shift upon a decrease of pressure. The roman numbers label different pressure phases.

observed as diagonal lines on the (001) surface. After increasing pressure beyond the range of phase II, the lines disappear completely. They occur again when pressure is reduced below ~6 GPa. Further decrease of pressure below ~4 GPa removes the lines again. As seen in Figure 11, some damage to the sample occurred but only upon decompression. However, the PE crystal remained intact over several loading and unloading cycles of pressure. It is worthwhile mentioning that the lines were not observed on other surfaces, that is, (010) and (100). This inference was made by viewing these planes through the diamond windows.

IV. Discussion

In PE crystals the Raman data clearly display three distinct regions of pressure dependencies. Below, we discuss possible changes induced in the crystal in each of these three regions.

IV.A. Pressure Range below 4.6 GPa: Phase I. At ambient conditions, the PE crystal has an ordered bct structure, with the following unit cell parameters: $a = 6.075$ Å ($\sqrt{2}a = 8.592$) and $c = 8.733$ Å. Because the compressibility along the [001] direction is considerably larger (~6 times) than that along the [100] direction, it is expected that with increasing pressure, p, the $c(p)$ parameter will eventually reach the value of $\sqrt{2}a(p)$. The high-pressure X-ray study of PE crystals reveals that this indeed occurs at ~0.28 GPa.[5] In such a case, PE crystals could be transformed to the fcc structure as observed at high temperatures. Although there was no sign of this transformation in high-pressure X-ray diffraction results, it was suggested that the PE structure could become metastable, and that a structural phase transition could be responsible for damaging the crystals when attempts were made to increase pressures above 1.15 GPa.[5]

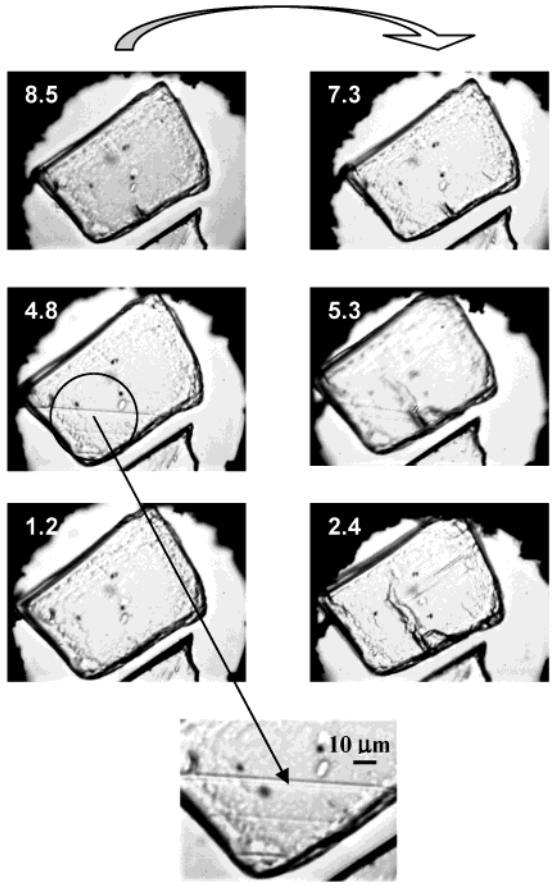

Figure 11. Optical images of the (001) plane of the PE crystal in the DAC at several pressures. The left and right panels represent images taken, respectively, upon an increase and a decrease of pressure. The bottom image shows a detail of the sample and the scale.

To attain the fcc structure, molecules of S_4 symmetry would have to undergo either internal rotations (e.g., about C−C and/or C−O bonds) or spatial rotations of molecules would have to occur to furnish the crystal as a whole with symmetry characteristics of a cubic system. It is expected that these transformations would generate a series of anomalies (e.g., discontinuity, broadening, or changes in modes multiplicity) in the spectra. However, it appears that all vibrational modes change continuously with pressure up to 4.6 GPa, showing no evidence for the suggested bct-to-fcc phase transition. In addition, the optical images of PE crystals taken at various pressures do not confirm any visible damage of the sample at pressures below 4.6 GPa (see Figure 11). Thus, the present results do not support the earlier suggestion of the phase transition in PE at about 0.5 GPa.[12, 13, 29]

As pressure increases, all internal and external modes shift to higher frequencies. Only OH-stretching modes show an exception to this general trend. The extent of the pressure-induced shifts varies among the modes. However, the OH and some CH vibrations seem to be, initially, the most affected by pressure. This may be due to the fact that these vibrations are associated with the terminal atoms, which are directly exposed to the reduction in intermolecular distances and, thus, to changes in intermolecular interactions. In contrast, the modes associated with the inner atoms display smaller shifts. However, among them the bending modes of the CCC-skeletal and CCO vibrations appear to be the most susceptible to pressure. This would suggest modification of the skeletal structure of the PE molecule by pressure. The available crystallographic data show

that the valency angles about the central C atom in the PE molecule are different, indicating that the surrounding C atoms do not form an ideal tetrahedron around the central C atom because of strong hydrogen bonding within the (001) planes.[5] A large red shift of the OH-stretching modes under pressure implies strengthening of hydrogen bonding and, thus, the enhancement of interactions in the (001) planes. Consequently, the initial elongation of molecules along the [001] crystal axis may be enforced further, affecting the frequencies of skeletal modes more than other modes. This directional deformation of molecules may also favor the activity of one symmetry species over the other ones. Conceivably, this effect may contribute to the observed initial increase of intensity of E-modes with pressure, in particular the external one. Because the compressibility along [001] is larger than in the (001) planes, the interlayer distance reduces more than the distance between the molecules in the planes. Thus, the differences in interactions in these two normal directions will gradually diminish and the anisotropy effects become less evident in the spectra at higher pressures. Finally, above ~4 GPa, a substantial decrease in frequency shifts observed on many of the modes indicates an increasing rigidity of the structure prior to the transition at 4.6 GPa.

Recently, an attempt was made to compute the vibrational spectra of PE under pressure.[29] Applying the Born−von Karman formalism and employing the structural data of ref 5, the frequencies of internal and external modes were calculated at pressures up to 1.15 GPa. These calculated results are contradicted strongly by our experimental data. First, all of the calculated shifts are several times larger than those observed in experiments. Second, many torsional, deforming, and all bending modes were calculated to have red shifts instead of the blue shifts observed in the data. Finally, the calculated shifts of the OH-stretching modes are extremely large, ~250 cm^{-1} GPa^{-1}, and are toward the blue instead of the red. These large disagreements indicate a significant difficulty with the computational effort in ref 29. The potential model, utilizing the harmonic approximation, used in these calculations is likely not applicable at high pressures.

IV.B. Pressure Range between 4.6 and 6.8 GPa: Phase II. The large array of new features occurring at 4.6 GPa indicates the onset of a phase transition. Because of the discontinuities in the spectra, pressure hysteresis, and time dependence associated with this transition, a first-order process is very likely. The hysteresis of this transition suggests the importance of strain and surface energy terms in the crystal free energy for this transition. Possibly the phase transition involves the nucleation and growth of a new phase within the old one. The difference in densities between the two phases would result in the new, inner phase being formed either under tension or compression within the old, outer phase, leading to different free-energy−pressure relations in the two directions of the transformation. In addition, a slow response of the crystal regarding completion of the transformation indicates the existence of an energy barrier between the two phases. Apparently, the set of parallel lines, on the sample surface, observed in phase II could be associated with the preferred directions of the new phase growth.

High pressures can destabilize the ambient structure by disturbing the balance of the intermolecular interactions and the intramolecular strains. Seemingly, at ~4.6 GPa the intramolecular strains do no longer support the increase of repulsive contribution in the total energy. Thus, the phase transition and/or changes in molecular conformations are expected to relieve the repulsive interactions. The examination of the internal modes just above 4.6 GPa indicates that PE molecules experience a reduced strain in phase II. Among a number of modes, the OH-stretching (ν_{26}, ν_{27}) and OH-torsion (ν_{10}, ν_{11}) modes seem to be subjected to the largest relief. This would imply that the phase transition at 4.6 GPa is brought about by the process leading to the weakening of hydrogen bonding, namely, by the increase of the H···O distance. Characteristically, the modes that experience the largest changes at the transition later show the smallest frequency shifts in phase II.

Another piece of information regarding the possible character of changes in the PE structure can be derived from mode splittings. The splitting of the nondegenerate internal modes as well as the degenerate ones could indicate the increase in the number of translationally nonequivalent molecules in the unit cell. The behavior of the external modes corroborates this conjecture. The shift of the external mode (ν_{L1}) is essentially continuous and smooth across the transition pressure. This response is strong evidence that the lattice structure is not altered significantly at the transition. Then, the appearance of the new external mode (ν_{L2}) and the apparent broadening of the ν_{L1} mode can be explained as follows. It is likely that at 4.6 GPa (in phase II) the unit cell of PE is enlarged, namely, doubled along both the *a*-axis and the *b*-axis direction. The enlargement can be caused by the generation of two nonequivalent molecules in the cell in terms of the strain they are experiencing. Two adjacent molecules could encounter different strains, for instance, by reorienting or tilting themselves in order to minimize the hydrogen-bonding interaction. Because the increase in the frequency of OH-stretching modes, at the transition, is about 10 cm^{-1}, the relative distortion between the two nonequivalent molecules should not be larger than a few degrees.[30, 31]

The doubling in real space implies a halving of the Brillouin zone (BZ) in the reciprocal space. Thus, the originally unavailable external modes at the original zone edge become available for scattering, since they become the zone-center modes after the folding. Therefore, the ν_{L2} mode and an apparent shoulder of the ν_{L1} mode can arise as a result of the BZ folding. At this point, it is not clear whether the ν_{L2} mode was the optical or the acoustic mode at the edge of the original BZ. However, the shoulder of the ν_{L1} mode could be the one derived from the ν_{L1} mode itself. Because ν_{L2} is observed for both orientations of the crystal, that is, for the beam normal and parallel to the [001] direction, the phonon responsible for this mode could also propagate in these directions. Therefore, the folding of the BZ and thus the doubling of the unit cell must occur at least along the [100] direction and, by symmetry, also along the [010] direction. The folding could occur also along the [010] direction. The available data are not sufficient to propose the specific structure of phase II.

IV.C. Pressure Range above 6.8 GPa: Phase III. The large changes in the spectra at 6.8 GPa indicate a major alteration of the crystal structure. Because the number of internal modes increases significantly and new modes occur in the vicinity of the E-modes, this would suggest changes in the molecular symmetry. Furthermore, the extremely large discontinuities in the OH-stretching modes at the phase transition imply a substantial modification in the arrangement of molecules. Striking changes in the external mode patterns supports this conjecture. An increased number of external and internal modes would indicate a modification of the PE structure accompanied by a further increase of the number of nonequivalent molecules in the unit cell, apparently by another factor of 2. However, a precipitous decline in the intensity of the external modes together

with an increasing background in this region suggests an alternative explanation.[32−34]

It seems that at sufficiently high pressure, namely 6.8 GPa, the increased energy of intermolecular interactions may modify the hydrogen bonds and favor the molecules to become orientationally disordered to permit shorter intermolecular separations. A number of factors, such as near vanishing of external modes and broadening of internal modes, point toward the disordered structure. From the splitting in the internal modes it may be concluded that the phase transition is also accompanied by conformational changes in the molecule. Furthermore, the broadening of internal modes implies a random arrangement and distortion, both within the molecules and between them.

V. Summary

The pressure effects on vibrational spectra of pentaerythritol single crystals have been reported for the first time. Care was taken to ensure that samples were subjected to hydrostatic pressures. Changes in Raman spectra including both the internal and external modes are determined up to 10 GPa. These studies do not confirm the postulated phase transition at ∼0.5 GPa reported earlier.[12,13,29] Instead, it is found that the structure at 1 atm becomes unstable at higher pressures. A number of abrupt changes in the spectra indicate strongly the onset of phase transitions at 4.6 ± 0.2 and 6.8 ± 0.3 GPa. These values differ from those obtained previously on PE powder.[16] It is proposed that the PE crystal can exist in three different phases in the pressure range up to 10 GPa. The phase I bct structure extends from ambient pressure to 4.6 GPa. From the splitting of internal and external modes observed, it is suggested that between 4.6 and 6.8 GPa the unit cell of PE is enlarged and the number of translationally nonequivalent molecules in it is doubled. Analysis of spectra above 6.8 GPa suggests that phase III could be disordered and associated with large softening of hydrogen bonding. Both transitions demonstrate considerable pressure hysteresis indicating first-order phase changes. Upon complete release of pressure, PE transforms back to phase I. These studies revealed new high-pressure phases of PE single crystals, providing the basis for further examinations. Clearly, X-ray diffraction measurements at high pressures are required to determine the exact structures of the new phases.

Acknowledgment. This work was supported by the ONR Grant N000149310369 and the DOE Grant DEFG0397SF21388. T.R.P. thanks Hoseo University for sabbatical leave support while performing this work.

References and Notes

(1) In *Molecular Systems under High Pressure*; Pucci, R., Piccitto, G., Eds.; North-Holland: Amsterdam, 1991.

(2) Decius, J. C.; Hexter, R. M. *Molecular Vibrations in Crystals*; McGraw-Hill Inc.: New York, 1977.

(3) Eilerman, D.; Rudman, R. *Acta Crystallogr., Sect. B* **1979**, *35*, 2458.

(4) Ladd, M. F. C. *Acta Crystallogr., Sect. B* **1979**, *35*, 2375.

(5) Katrusiak, A. *Acta Crystallogr., Sect. B* **1995**, *51*, 873 and references therein.

(6) Hvoslef, J. *Acta Crystallogr.* **1958**, *11*, 383.

(7) Llewellyn, F. J.; Cox, E. G.; Goodwin, T. H. *J. Chem. Soc.* **1937**, 883.

(8) Wyckoff, R. W. G. *Crystal Structures*, 2nd ed.; Interscience: New York, 1966; Vol. 5.

(9) Semmingsen, D. *Acta Chem. Scand. A* **1988**, *42*, 279.

(10) Chandra, D.; Fitzpatrick, J. J.; Jorgensen, G. *Adv. X-Ray Anal.* **1989**, *28*, 353 and references therein.

(11) Ramamoorthy, P.; Krishnan, K. *Indian J. Pure Appl. Phys.* **1996**, *34*, 341.

(12) Nitta, I.; Watanabe, T. *Bull. Chem. Soc. Jpn.* **1938**, *13*, 28.

(13) Frolov, A. P.; Vereshchagin, L. F.; Rodionov, K. P. *Fiz. Tverd. Tela* **1962**, *4*, 1608.

(14) Zhorin, V. A.; Maksimychev, A. V.; Kushnerev, M. Y.; Shashkin, D. I.; Enikolopyan, N. S. *Zh. Fiz. Khim.* **1979**, *53*, 2772.

(15) Hamann, S. D.; Linton, M. *Aust. J. Chem.* **1976**, *29*, 1825.

(16) Bhattacharya, T.; Sharma, S. M. *J. Phys.: Condens. Matter* **2002**, *14*, 10367.

(17) Barnett, J. D.; Block, S.; Piermarini, G. J. *Rev. Sci. Instrum.* **1973**, *44*, 1.

(18) Dreger, Z. A.; Gruzdkov, Y. A.; Gupta, Y. M. Unpublished work.

(19) McLachlan, R. D.; Carter, V. B. *Spectrochim. Acta A* **1971**, *27*, 853.

(20) Marzocchi, M. P.; Castellucci, E. *J. Mol. Struct.* **1971**, *9*, 129.

(21) Ramamoorthy, P.; Krishnamurthy, N. *Spectrochim. Acta, Part A* **1997**, *53*, 655.

(22) Camargo, F.; Lemos, V. *J. Raman Spectrosc.* **1990**, *21*, 123.

(23) Wang, X. B.; Shen, Z. X.; Tang, S. H.; Kuok, M. H. *J. Appl. Phys.* **1999**, *85*, 8011.

(24) Mammone, J. F.; Sharma, S. K.; Nicol, M. *J. Phys. Chem.* **1980**, *84*, 3130.

(25) Vinogradov, S. N.; Linnell, R. H. *Hydrogen Bonding*; Van Nostrand Reinhold Company: New York, 1971.

(26) Reynolds, J.; Sternstein, S. S. *J. Chem. Phys.* **1964**, *41*, 47.

(27) Moon, S. H.; Drickamer, H. G. *J. Chem. Phys.* **1974**, *61*, 48.

(28) Hamann, S. D.; Linton, M. *Aust. J. Chem.* **1975**, *28*, 2567.

(29) Ramamoorthy, P.; Rajaram, R. K.; Krishnamurthy, N. *Cryst. Res. Technol.* **2001**, *36*, 169.

(30) Lippincott, E. R.; Schroeder, R. *J. Chem. Phys.* **1955**, *23*, 1099.

(31) Schroeder, R.; Lippincott, E. R. *J. Phys. Chem.* **1957**, *61*, 921.

(32) Shuker, R.; Gammon, R. W. *Phys. Rev. Lett.* **1970**, *25*, 222.

(33) Winters, R. R.; Hammack, W. S. *Phys. Rev. B* **1996**, *53*, 14089.

(34) Rao, R.; Sakuntala, T.; Godwal, B. K. *Phys. Rev. B* **2002**, *65*, 054108.